Journal of Fluorescence
https://doi.org/10.1007/s10895-023-03312-1

RESEARCH

Thermal and Nonlinear Optical Properties of Sudan III

Amir Hussein Ali[1] · H. A. Sultan[1] · Qusay M. A. Hassan[1] · C. A. Emshary[1]

Received: 16 May 2023 / Accepted: 13 June 2023

Abstract
We report the experimental and theoretical study of the diffraction patterns (DPs) and thermal properties of Sudan III. DPs are used in the calculation of the Sudan III nonlinear refractive index (NLRI), n_2. As high as $n_2 = 7.69 \times 10^{-6}$ cm^2/W is obtained. The study of the Sudan III thermal conductivity, TC, shows the reduction of the TC against the increase of the Sudan III temperature. The property, all-optical switching (AOS), is studied in details, both static and dynamic ones, using two, cw, visible, single mode laser beams of wavelengths 473 and 635 nm.

Keywords Sudan III · Thermal properties · Nonlinear optical properties · Diffraction patterns · All-optical switching

Introduction

Great interest has been expressed in the recent years, to study available materials, improved available materials, and synthesized new materials [1–15], due to the potential of enhancing their nonlinear optical (NLO) properties that leads to photonic devices use. Number of properties of materials have been studied simultaneously viz., thermal diffusivity [16], spectroscopic and thermal [17], thermally and optically induced change of structure, linear and NLO properties [18], nonlinear and thermo-optic parameters [19], thermal lens [20], thermo-optic coefficient [21, 22], medical, thermal and laser damage [23], optical and thermal [24], structural, thermal, and optical properties [25], thermal / spectral and optical enhancements [26, 27], etc.

Recently intense efforts have been directed towards the study of the NLO properties of variety of media by Jeyaram et al. viz., basic violet 3 solution via Z-scan techniques [28], novel organic compound [29], organic compound [30], and a Schiff base via variety of techniques [31] for variety of NLO applications. In addition, our group presented, new materials during the past six years, that possess high NLO properties, which demonstrated their potential for use as optical limiters and switches [32–38].

Sudan dyes are available in different types i.e., Sudan orange G, Sudan black B, Sudan brown RR, Sudan red B, Sudan red 7B, Sudan (I-IV), and Sudan red G [39–41]. These types of dyes have received vast interest including the optical properties viz., under the effect of solvents [42]. Sudan III dye doped polymer optical limiter behavior [43], vibrational studies investigation of structure and NLO properties [44], use in optical sensor applications [45], photo-induced dichroism [46], Sudan III/PVK film composite physical structure [47], and optical properties [48].

We believe that, the diffraction patterns and thermal properties of Sudan III dye have not been studied previously. Therefore, in the current work, we will study the thermal properties of Sudan III dye where the thermal conductivity (TC) of Sudan III at different temperatures were studied. By excitation with a visible, cw, laser beam, the NLO properties of Sudan III dye were also investigated. The nonlinear refractive index (NLRI), n_2, of Sudan III was determined using diffraction patterns (DPs) method. A theoretical simulation of experimental results was carried out using Fresnel-Kirchhoff (F.K.) integral. The property, all-optical switching (AOS), of the Sudan III was tested using 473 nm and 635 nm laser beams.

✉ Qusay M. A. Hassan
qusayali64@yahoo.co.in

[1] Department of Physics, College of Education for Pure Sciences, University of Basrah, Basrah 61001, Iraq

Published online: 20 June 2023

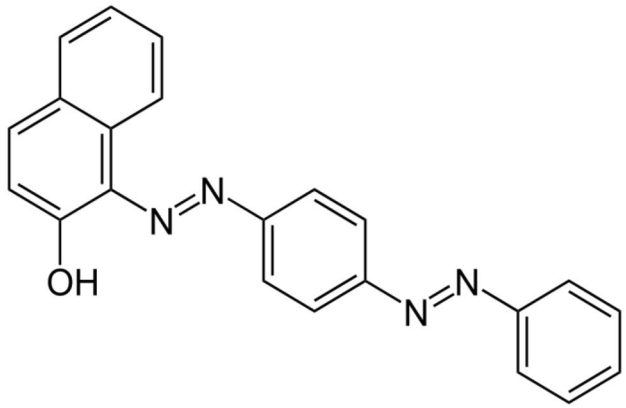

Fig. 1 The chemical structure of Sudan III

Experimental

Sample

Sudan III and dimethylformamide (DMF) used in the current study were purchased from Sigma Aldrich. The chemical structure of Sudan III is presented in Fig. 1. Its chemical formula, melting point, and molar mass are $C_{22}H_{16}N_4O$, 199 °C, and 352.397 g/mol, respectively. This dye is characterized by its crystalline appearance and its color is red-brown. A certain amount of Sudan III was dissolved in DMF to obtain a concentration of 5 mM. This concentration was used to carry on all the experiments mentioned in this work.

Experimental Set-Up

Two routes were followed in studying the properties of Sudan III.

NLO Properties Experiments

The NLRI, n_2, of Sudan III dye was calculated by generation of DPs using the set-up illustrated in Fig. 2. The diffraction patterns temporal variation and their dependence on power input studies were carried out. The excitation beam is obtained by a laser device with power output varied between zero and 66 mW, cw beam of wavelength 473 nm. Spot size radius of the laser beam was 1.5 mm (at e^{-2}) focused to a spot of 19.235 μm size by a glass, convex, 5 cm focal length lens.

The 1 mm thickness sample cell was situated at the lens focus, a 30×30 cm semitransparent screen was used where the DPs were recorded by a digital camera with exposure time of 1/32 sec. The AOS was carried out using two cw laser beams of wavelengths 473, and 635 nm having the same spot size (1.5 mm) via the technique cross-passing [49–51]. The two beams were focused at the sample cell by two, 20 cm, convex lenses focal lengths where the spot sizes of the two lasers beam become 76.941 μm and 103.293 μm at their foci respectively. The beam 473 nm was taken as the controlling beam while the 635 nm beam considered as the controlled one as shown in Fig. 3. The diffraction patterns formed on a 60×60 cm semitransparent screen.

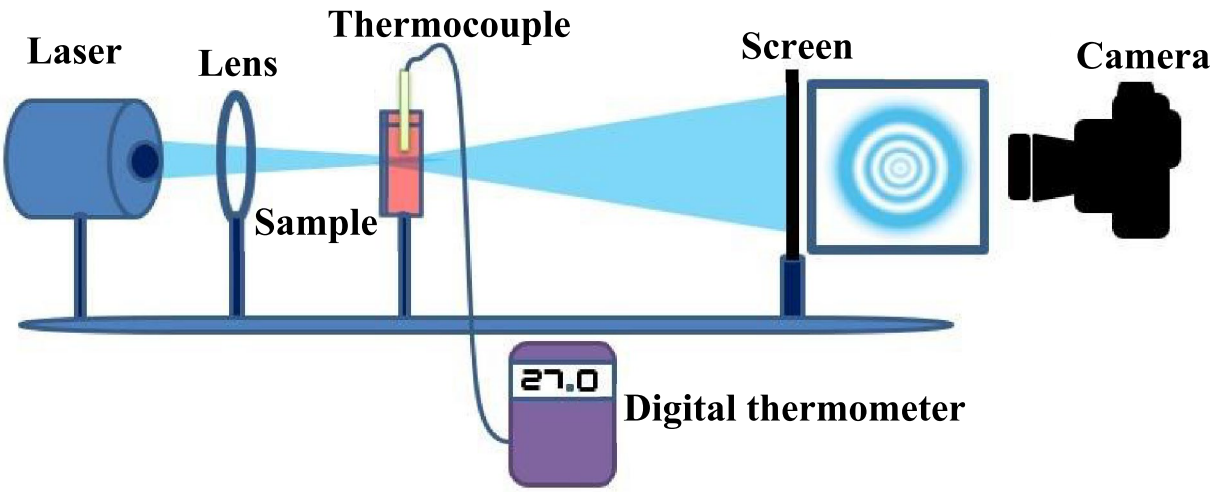

Fig. 2 Diagrammatic set-up for obtaining DPs

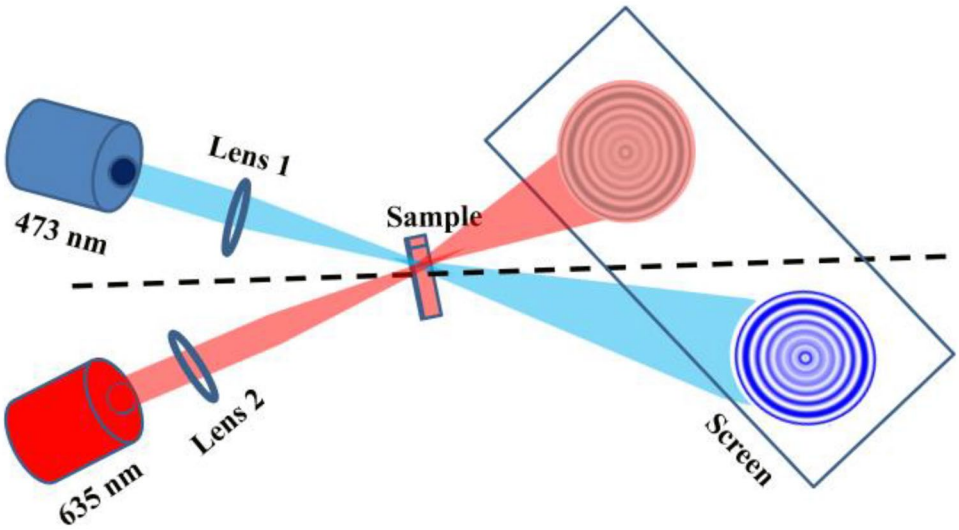

Fig. 3 Diagrammatic set-up for obtaining AOS

Sudan III temperature in the presents of laser beam was measured using a thermocouple type digital precision instruments HT-9815 thermocouple thermometer (-200 ^{0}C-1370 ^{0}C) as shown in Fig. 2.

Thermal Conductivity Measurement

TC is considered vital for the physical studies and engineering applications. Heat transfer is a process by which heat is transferred from one region to another one in the direction of temperature fall. To calculate the TC of a material the following (Fourier law) mathematical formula is used [52]

$$\dot{Q} = -kA\frac{dT}{dx} \tag{1}$$

$\dot{Q}$ is the amount of heat flow through the sample per unit of time, A is the surface area normal to heat flow, dT is the difference in temperature between the two faces of the sample, dx is the sample thickness and K is the TC. The classical method for thermal conductivity measurement is Lee's disk method [53]. The classical method of Lee has undergo some modifications [54]. However, in the present work, a new modification has been introduced to measure the TC of Sudan III. Figure 4 shows the TC measurement set-up.

Two disks of 2.3 cm diameter have been used, disk 1 and disk 2. Disk 1 has 2.3 cm height whereas disk 2 has height of 1.1cm. The disks material is made of Brass. To insulate the side walls of the disks against the environment, the two disks have been wrapped around by insulating paper. For measurement purpose, a powder of Sudan III was pressed to make suitable hard disk sample of thickness of 1.6 mm. The sample has been placed between the two disks. Disk 1 has been heated by adjustable heater. Three holes of few millimeters deep inside the disks were made to connect the thermocouples, two holes at the two surfaces of disk 1 and one hole at the first face of disk 2 immediately after the sample. The three holes temperatures have been recorded and denoted as T1, T2 and T3 respectively as illustrated in Fig. 4. It is well known that under steady heat transfer condition, the heat flow rate through disk 1 and the sample is the same. This fact has been used in Fourier's law to measure the TC of the sample. The TC has been measured for a range of temperatures as shown in Fig. 5. The measurements has revealed that TC decreased as the temperature of the sample increased.

Linear Absorption Coefficient Measurement

The linear absorption coefficient, α_i, of Sudan III at wavelength, λ_i, was measured at RT using a spectrophotometer

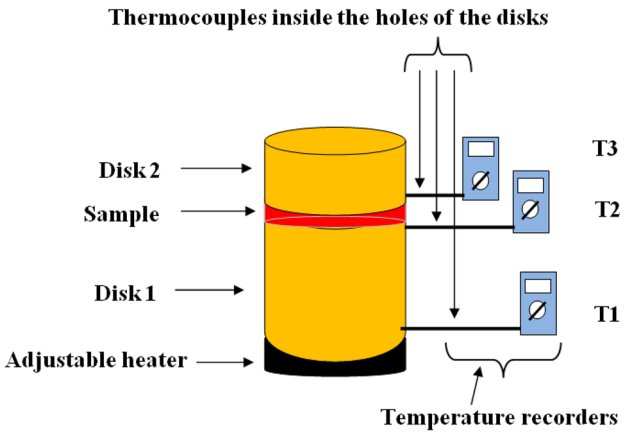

Fig. 4 Sketch of the thermal conductivity measurement device

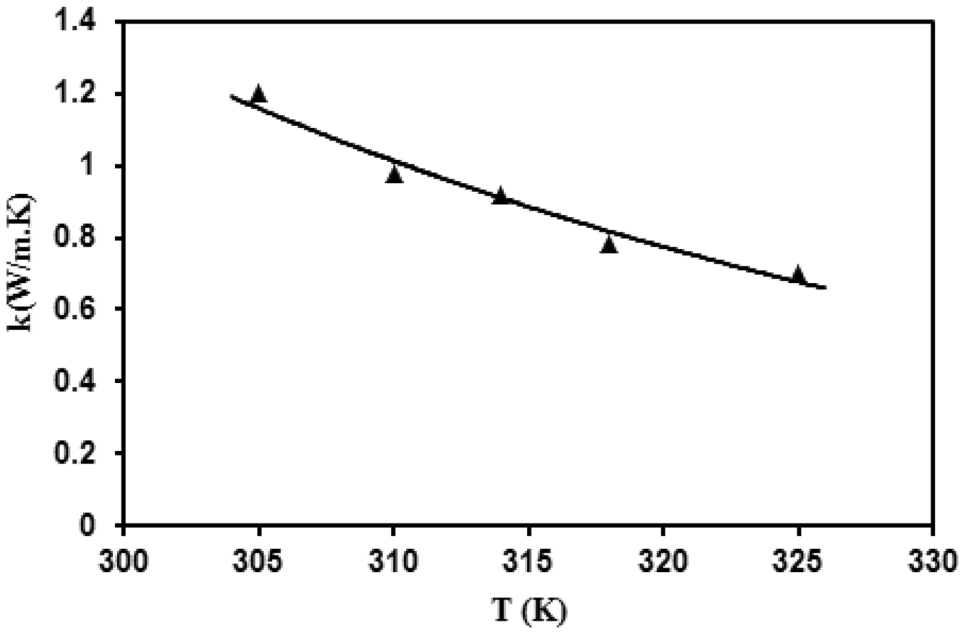

Fig. 5 TC versus temperatures of Sudan III

type (England 6800) where Fig. 6 shows the absorbance (A) measured in the UV-visible region. To calculate α_i, the following mathematical formula was used [55]

$$\alpha_i = 2.303\frac{A}{d} \quad (2)$$

A is sample absorbance and d its thickness. The values of α_{473} and α_{635} are 11.43 and 1.21 cm^{-1} respectively.

Results

Diffraction Patterns

Figure 7 shows a chosen DP temporal variation as the laser beam traversed through the Sudan III obtained by changing the cw behavior of the laser beam into pulse (square) one using a frequency generator the TTL function. It is

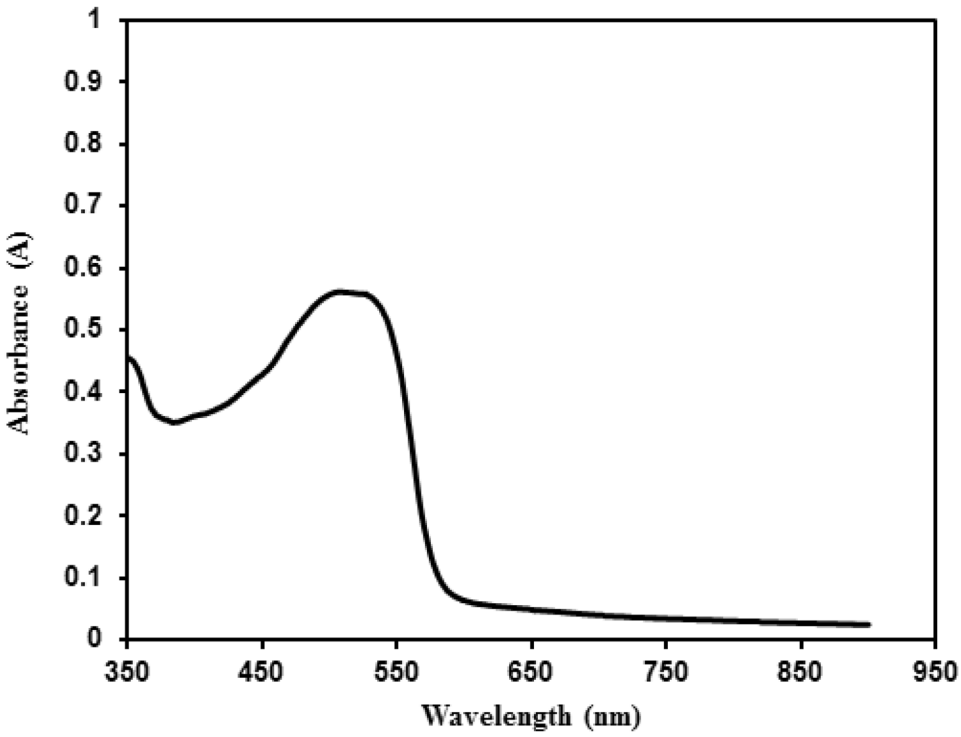

Fig. 6 Absorbance (**A**) spectrum of sudan III solution

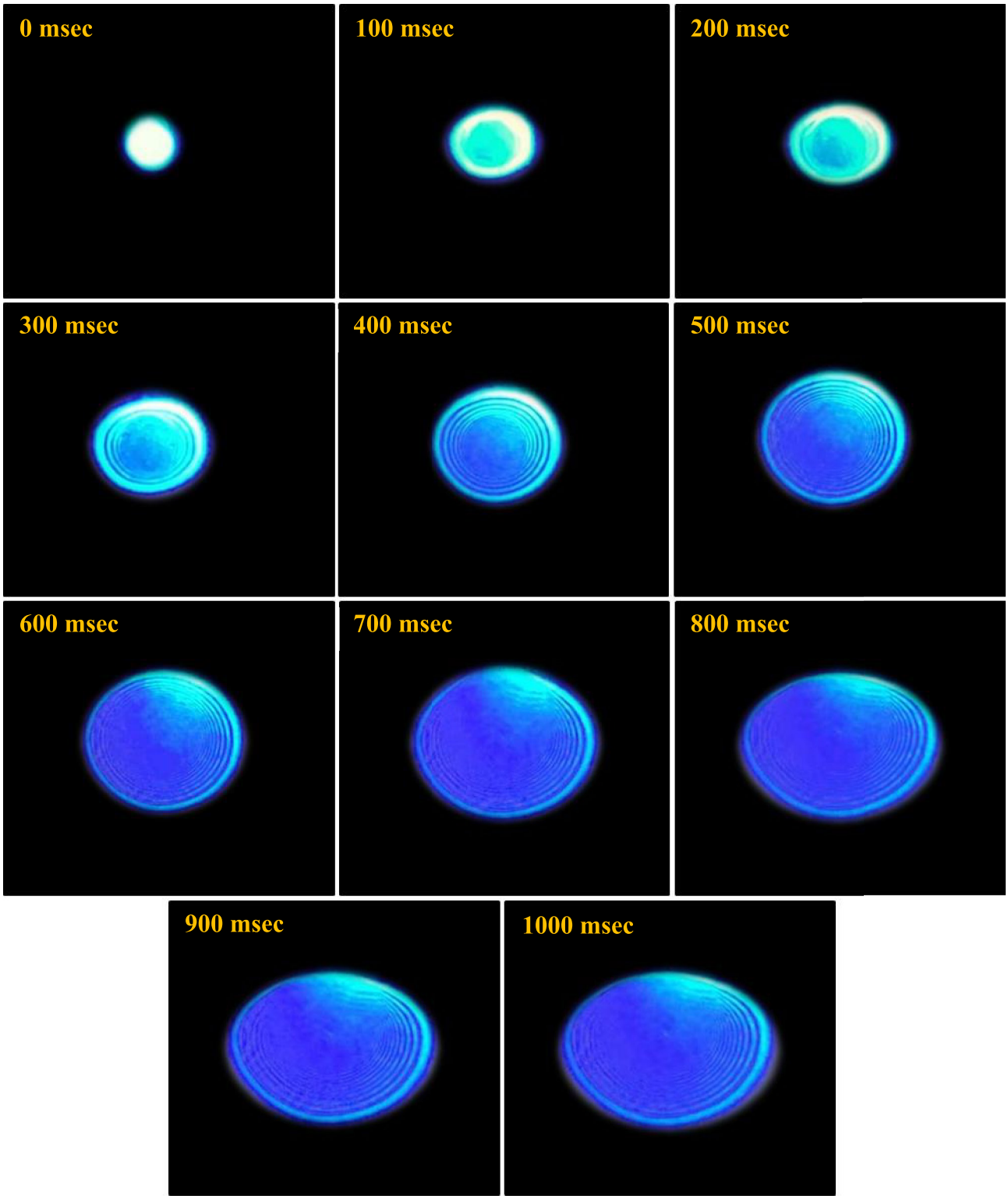

Fig. 7 Temporal evolution of DPs as the laser beam passes through Sudan III, with power 62 mW

seen that at initial time the shape of the beam spot as it falls on the screen is a small bright spot with no rings as if the sample is absent.

As time lapse the spot quickly increases in area due to self-defocusing (SDF), until the spot breaks into rings which was symmetric in the x-y plane with respect to the

propagation z- axis. As time lapse the pattern started losing symmetry in its upper half due to thermal convection current so that it's upper half grew in smaller ratio compare to the lower one.

Finally, the asymmetric pattern reaches a steady state. At low power input, laser beam draws a bright spot on the screen. With the increase of power input, the beam area increases due to SDF as seen in Fig. 8. With the continuously increased power input, the spot breaks into rings which increases in area, in number and asymmetry, following the same behavior noticed in Fig. 7. For a chosen input power of 37 mW, Fig. 9 shows the effect of concentration of Sudan III on the DPs where it can be seen that the DP started as a bright spot that increases in area then breaks into rings. A behavior mimic the effect of input power or time evolution of the DPs. When the concentration increased so does the number of Sudan III molecules that increases the temperature locally so does the DP evolute with concentration. The Sudan III temperature and number of rings in the DP are studied when DP resulted where it can be seen in Fig. 10 these quantities increases monotonically against power input. The increase of number of rings with laser beam power input agrees well with the conclusion reached in subsection "Linear Absorption Coefficient Measurement", i.e., with the power input increased the absorbed amount of energy increased, so that the refractive index (RI), increases which increases the phase of the laser beam.

Calculation of Sudan III NLRI

The DPs were used in the calculation of Sudan III NLRI, n_2, where it is believed that number of rings resulted at the highest incident power input [56] so that

$$n_2 = \frac{\pi\omega^2}{2}\frac{N\lambda}{Pd} \tag{3}$$

ω is the beam radius at entrance of the sample, P is the incident laser beam power, and λ is the beam wavelength. For P = 62 mW, N =14, d =0.1 cm,λ = 473 nm,ω =19.235 μm so that $n_2 = 7.693\times10^{-6}$ cm^2/W for Sudan III. Such high n_2 value is higher than so many materials [56–64] as shown in Table (1).

All-Optical Switching

Two laser beams of wavelengths 473 and 635 nm were used. First beam, 473 nm, is the controlling or excitation beam while the second one is the controlled, 635 beam. As can be seen from subsection "Linear Absorption Coefficient Measurement" the Sudan III have low absorption coefficients at 635 nm wavelength, so that low energy was absorbed and less heat generated so that no rings appeared as seen in Fig. 11X1(a), when 635 nm beam imping alone

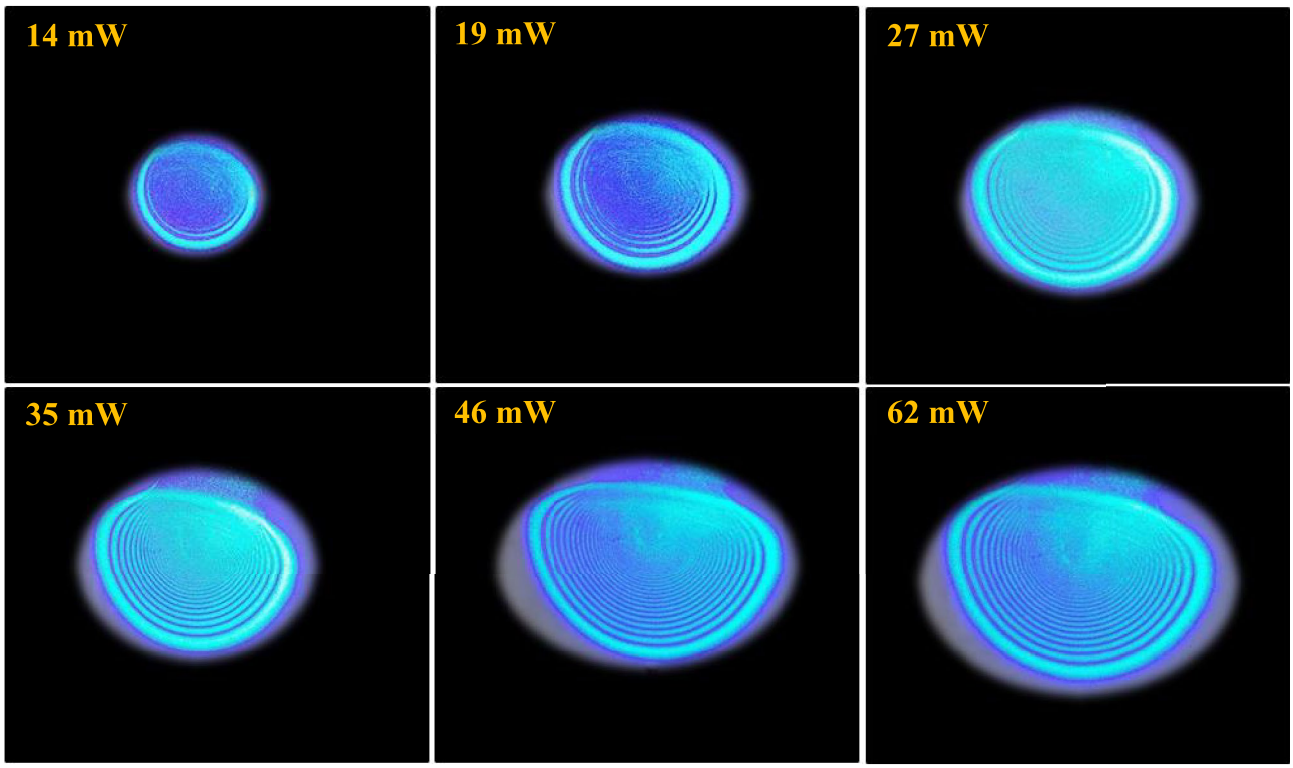

Fig. 8 Variations of the DPs against input power when the laser beam passes through Sudan III

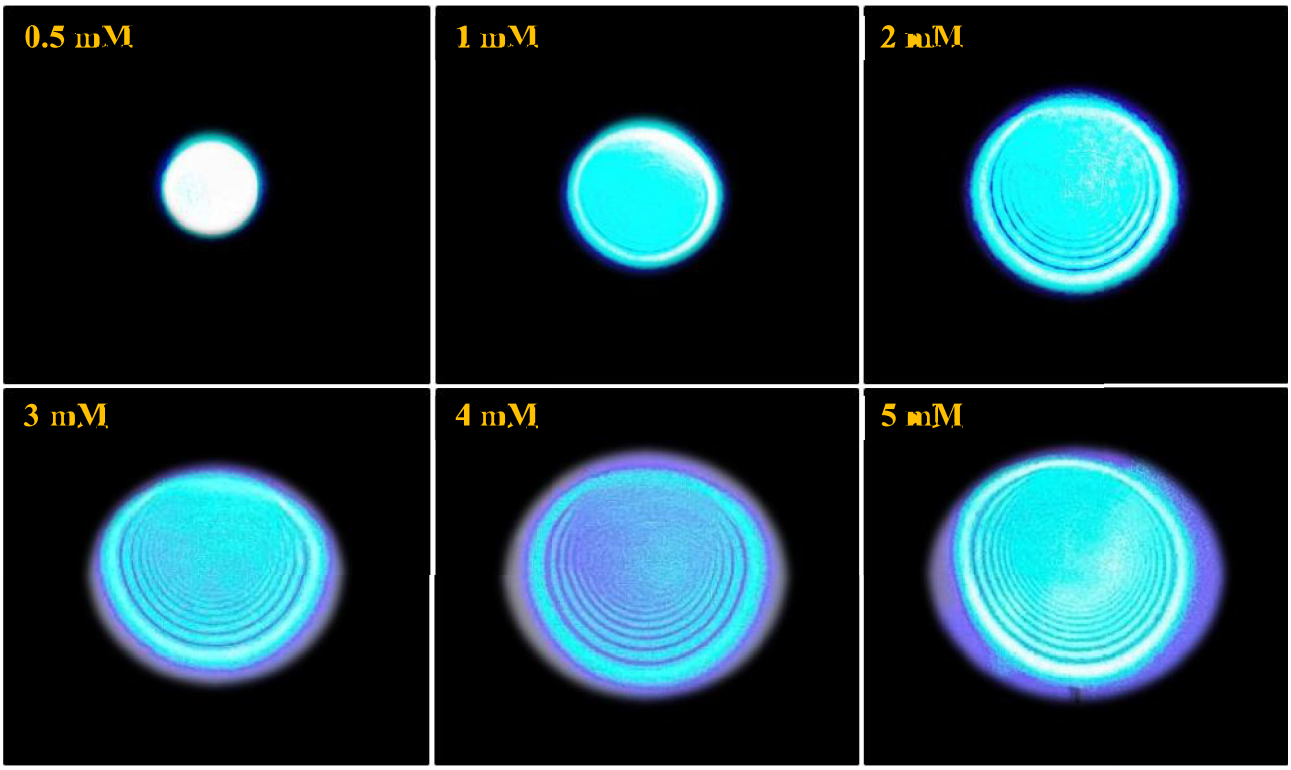

Fig. 9 Variations of the DPs against Sudan III concentration at power input 37 mW

on Sudan III. When the 473 nm beam with moderate power input imping on Sudan III alone DPs resulted as seen in Fig. 11X1(c).When the two beams imping on Sudan III, simultaneously, two DPs resulted one due to the controlling beam and one for the controlled beam where it can be seen that one new patterns resulted for the 635 nm beam due to the 473 nm controlled beam as seen in Fig. 11X1. When the controlling beam power increased, its DPs increased in

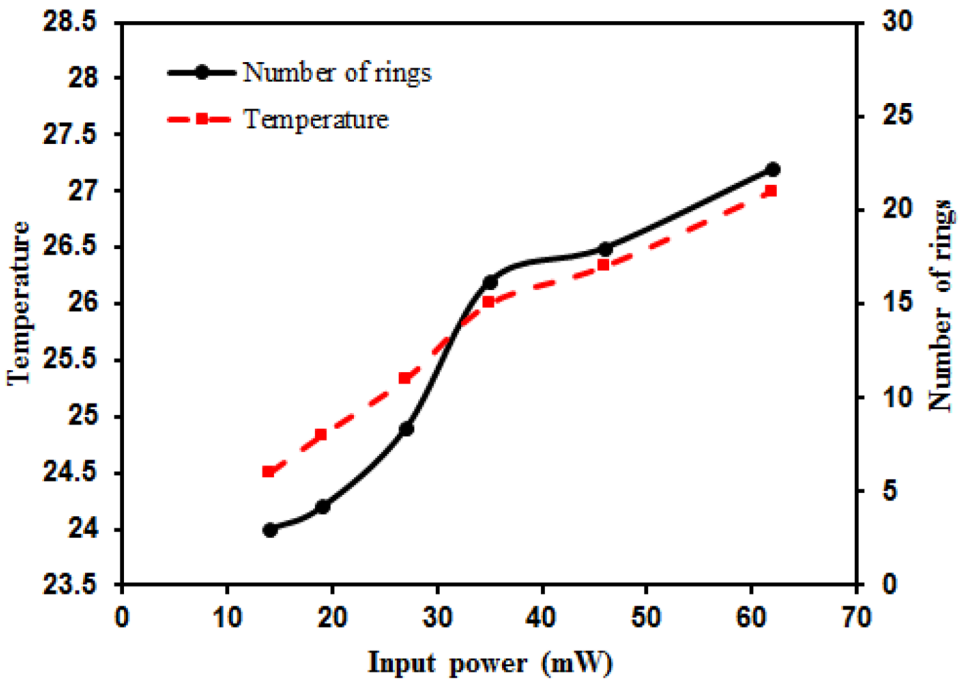

Fig. 10 Variations of Sudan III solution temperature (°C) and number of rings, N, against input power of laser beam

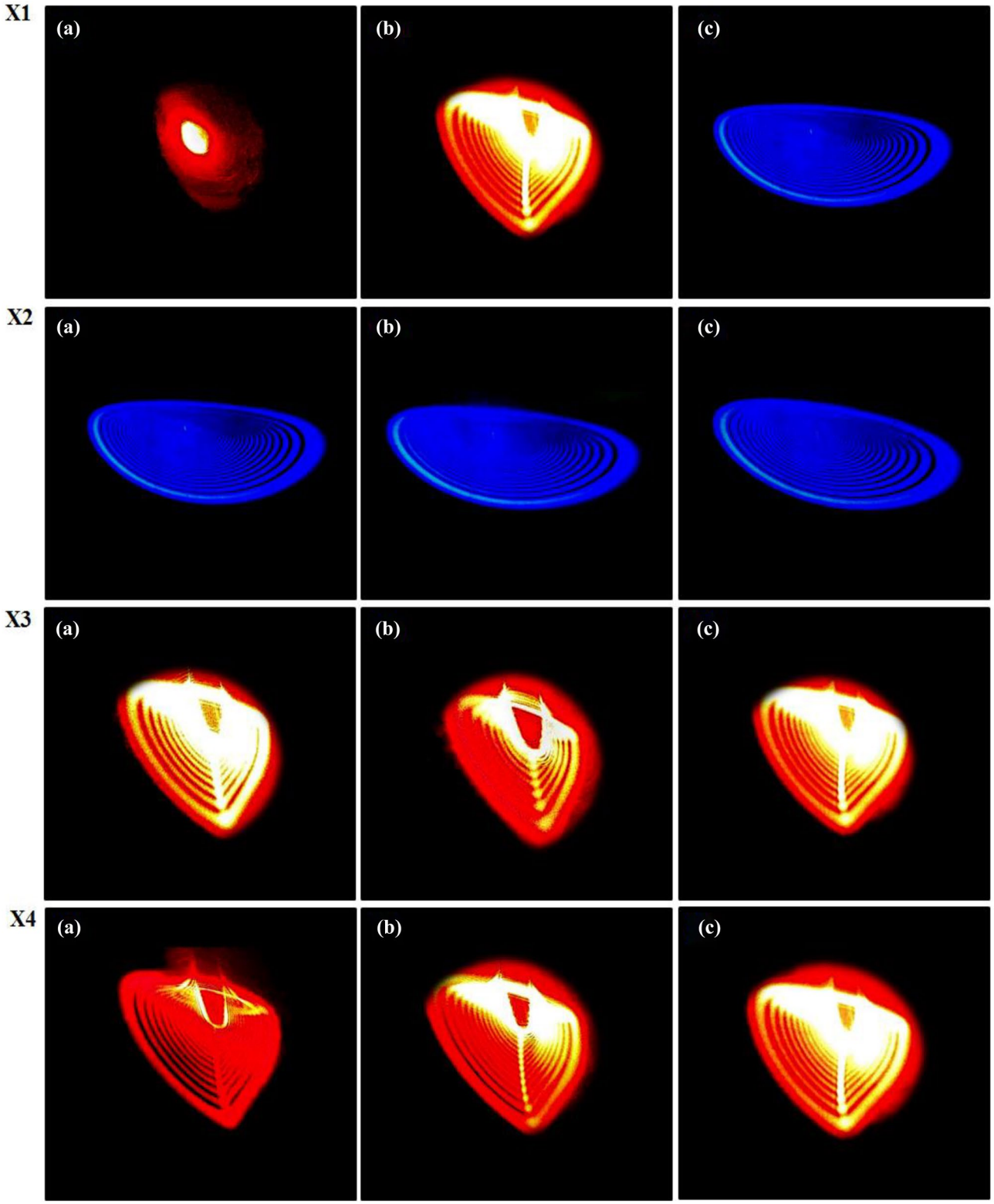

Fig. 11 Static AOS. When the 635 nm beam passes in Sudan III solution alone and its power increased from zero to 50 mW a bright spot appeared as seen in Fig. 11X1(**a**). When the 473 nm beam with low power, DPs appeared as seen in Fig. 11X1(**c**), and red rings appeared as seen in Fig. 11X1(**b**) as a result of the XPM effect of the 473 nm against the 635 nm. Effect of 473 nm power on the 635 nm rings is seen in Fig. 11X2 and on its rings are shown in Fig. 11X3, The effect of 635 nm beam on its rings is shown in Fig. 11X4

area, in number of rings, intensity, and asymmetry as seen in Fig. 11 X2, while the other 635 nm beam DPs area, number of rings, and asymmetry increase, as shown in Fig. 11 X3. When increasing the intensity of the 635 nm beam input power it increases its DP intensity only and it has no effect on the DPs of the 473 nm as seen in Fig. 11X4. The enhancement of the new DPs due to the 635 nm is due to the phenomena cross-phase modulation (XPM), an effect noticed as early as 1987 [65–70]. Figure 12 shows temporal variation of the results shown in Fig. 11 where the input laser beam power (473 nm) changed into pulse one by changing the controlling beam output power of 473 nm,

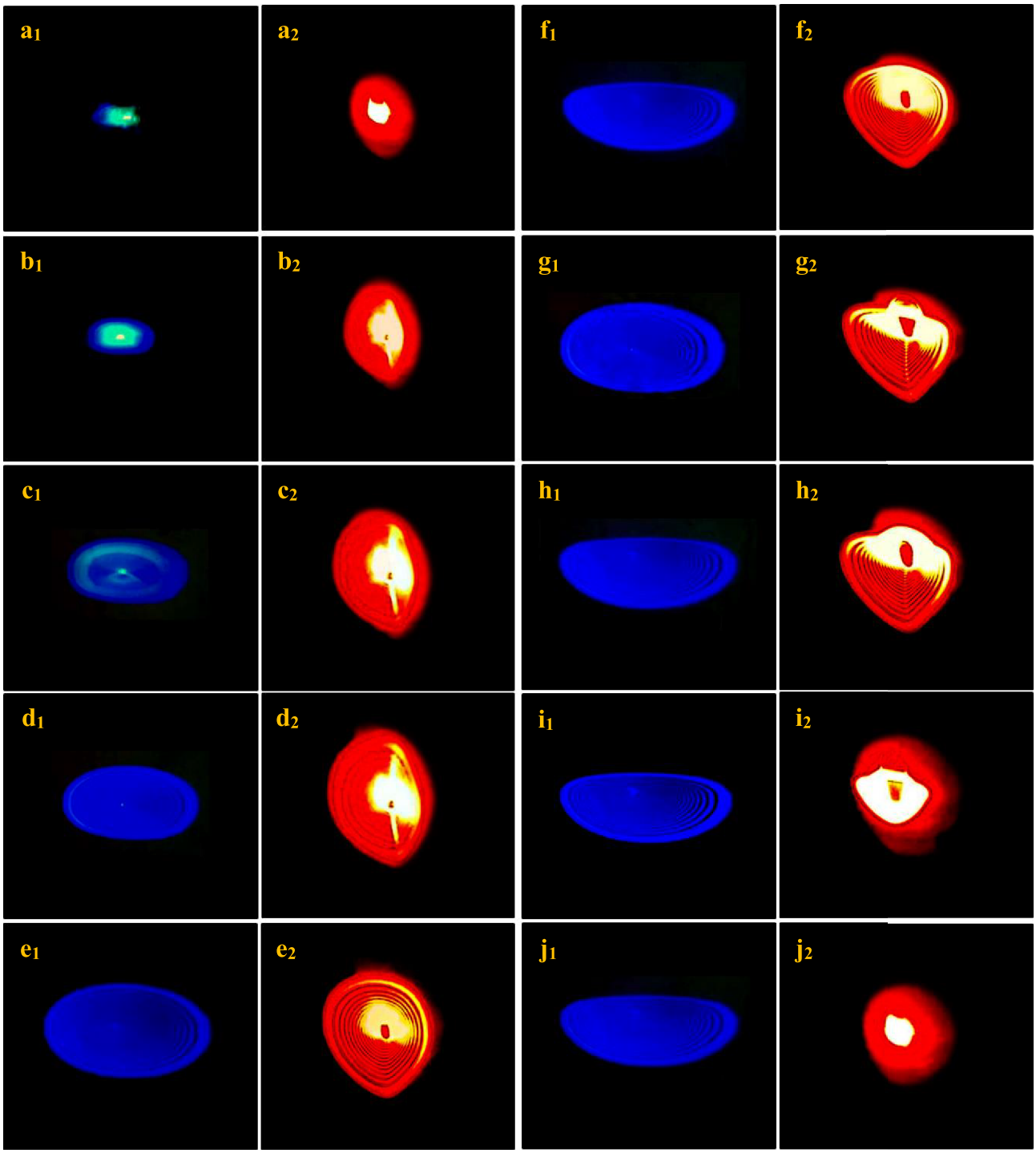

Fig. 12 Dynamic AOS where the controlled red 635 nm patterns followed the evolution of the controlling blue 473 nm patterns in Sudan III solution

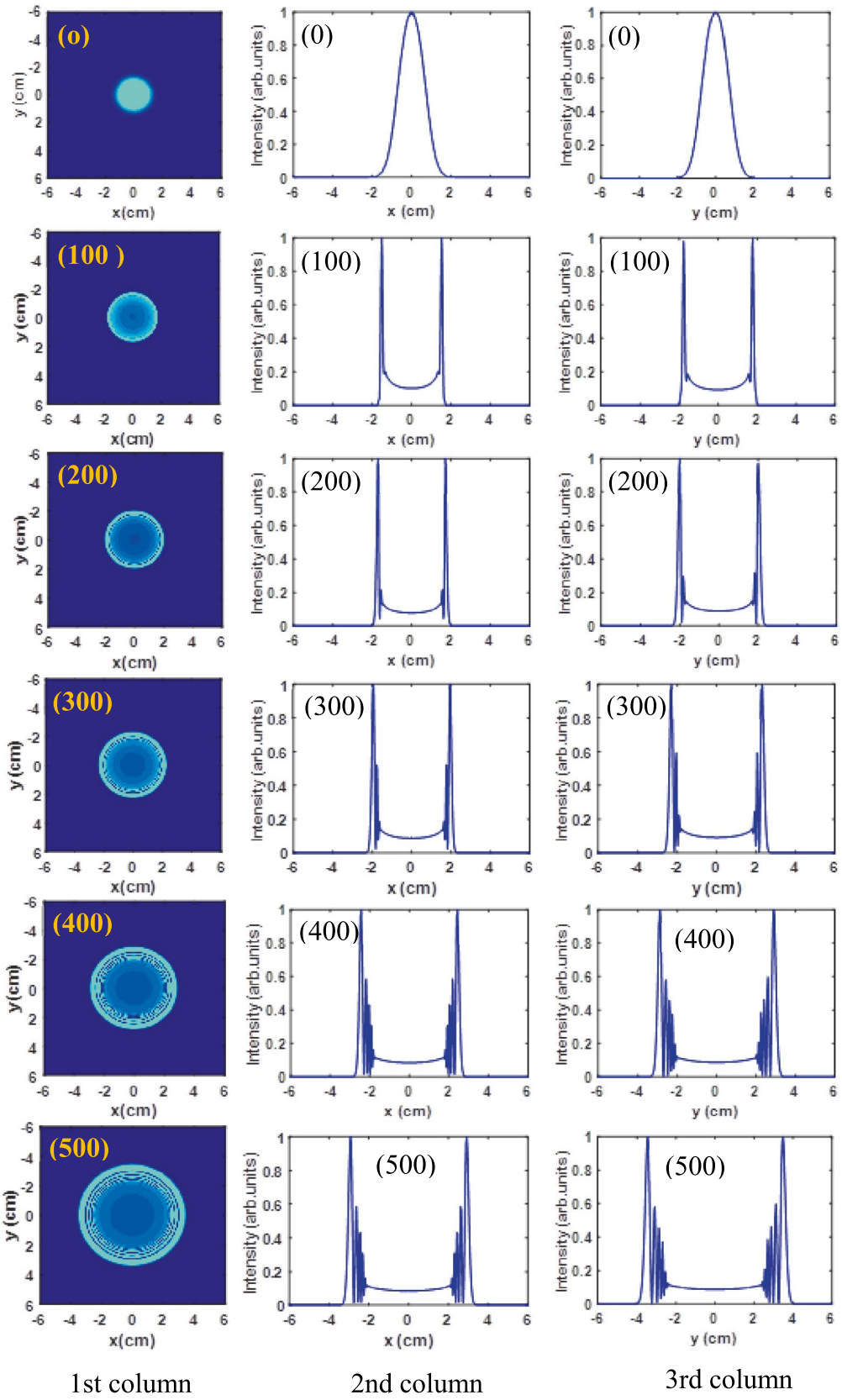

Fig. 13 Simulation results of the 2D temporal variations (0 -1000 msec) of a chosen (1st c.) DPs shown in Fig. 7, 1-D intensity variation against x-axis (2nd c.) and against y-axis (3rd c.) in Sudan III solution

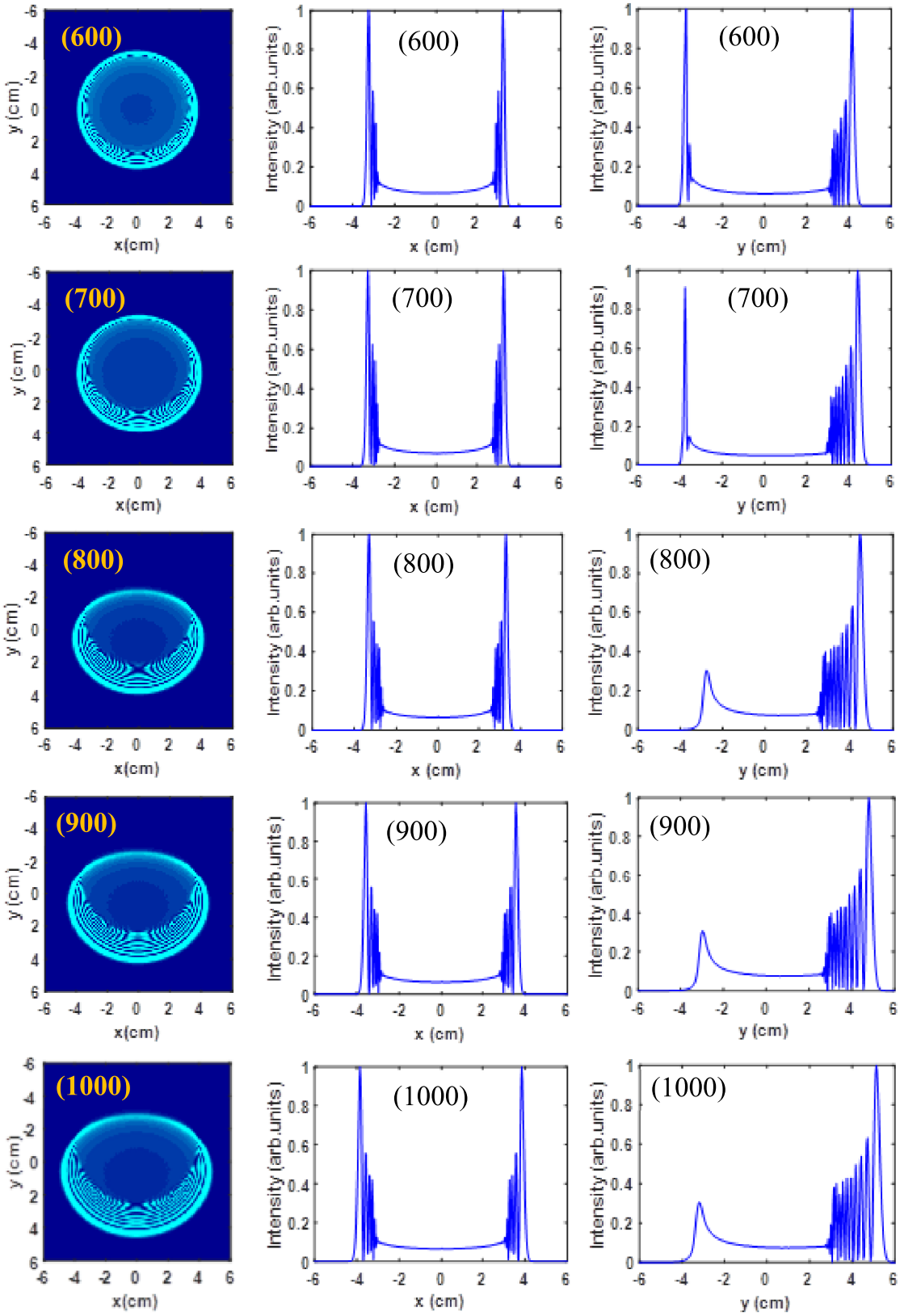

Fig. 13 (continued)

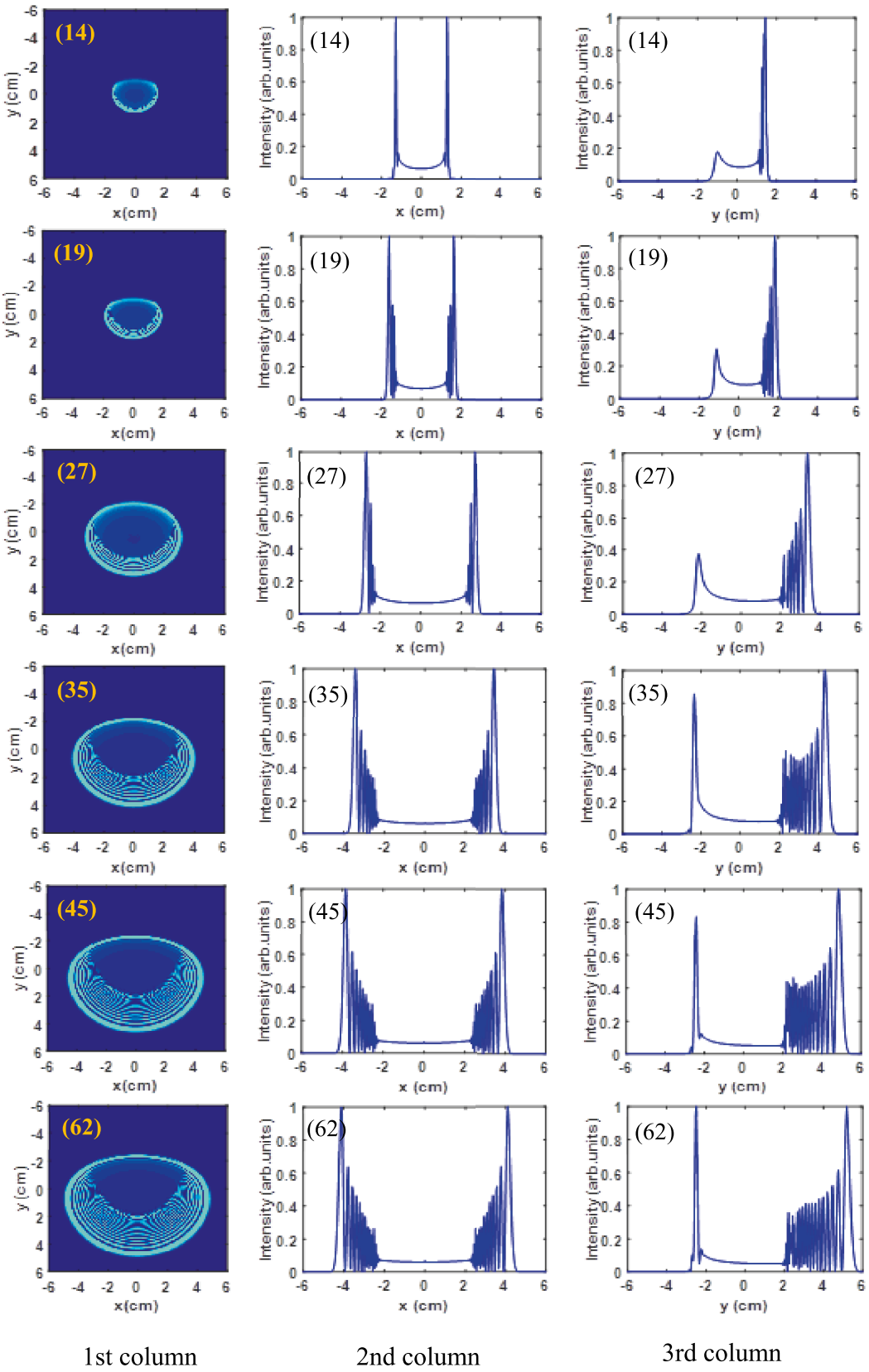

Fig. 14 Simulation results of variation of diffraction against input power (14-62 mW) (1st c.), the 1-D intensity variation against x-axis (2nd c.) and against y-axis (3rd c.), in Sudan III solution

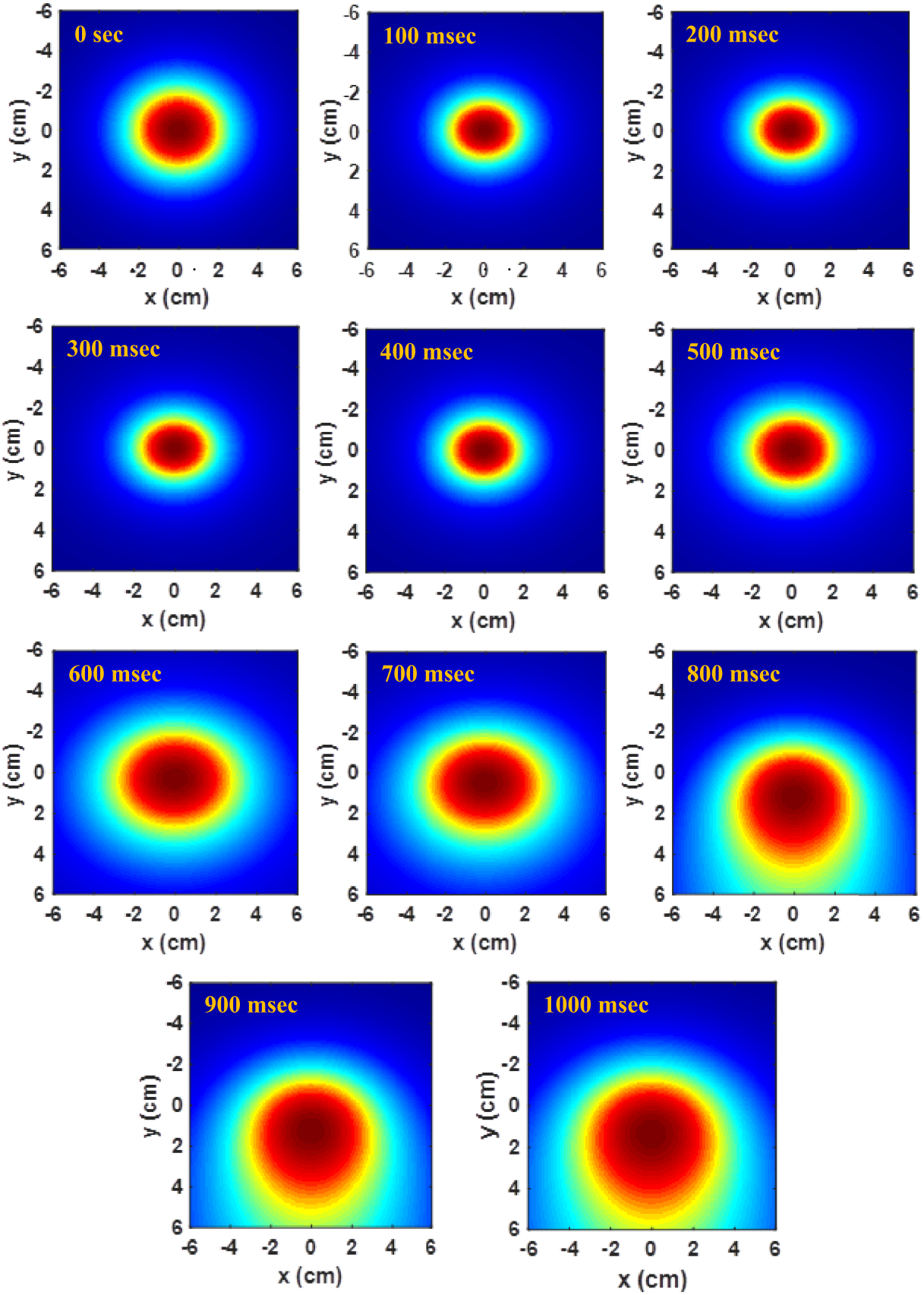

Fig. 15 Simulation results of the 2-D temporal variation of beam phase at input power 62 mW, in Sudan III solution

by using a frequency generator and using the TTL function that change the 473 nm laser beam into pulsed (square) one. This method changed the enhanced 635 nm pattern due to the XPM into pulse one i.e., the effect become dynamical all-optical switching.

Simulation of DPs

To simulate the DPs formed in subsection "Diffraction patterns" due to the passing of the cw laser beam, we need to develop an equation based on the F. K. integral and Fraunhofer approximation. In determining the DPs, it is supposed that a horizontal, cw, laser beam with Gaussian profile enter the sample cell of thickness, d, where the complex amplitude of the laser beam enters the sample cell from left along the z-direction and vary spatially can be written in the (x-y) plane as follows:

$$E(x,y,t,z=0)=\left(\frac{2P}{\pi\omega^2}\right)^{\frac{1}{2}}\exp\left(-\frac{x^2+y^2}{\omega^2}\right)\exp\left(-ik\frac{x^2+y^2}{2R}\right) \tag{4}$$

P is the incident laser beam power on the sample, k is the light wave vector (=2 π/λ), r is the perpendicular distance from the beam center and R is the beam wave front radius. Based on the amount of laser beam absorbed energy by the medium, the later temperature increased with Gaussian profile. Based on the medium thermal properties such as thermo-optic coefficient diffusivity, conductivity, etc., that lead to the medium RI variation, n(x,y,t), the laser beam suffers variations of its initial phase, Δφ(x, y, t), so that equation (4) becomes:

$$E(x,y,t,z)=\left(\frac{2P}{\pi\omega^2}\right)^{\frac{1}{2}}\left(-\frac{\alpha d}{2}\right)\exp\left(-\frac{x^2+y^2}{\omega^2}\right)\exp\left(-ik\frac{x^2+y^2}{2R}\right)\exp(i\Delta\varphi(x,y,t)) \tag{5}$$

The x and y spatial variables are at the sample plane becomes x' and y' at the screen. The laser beam intensity on the screen via F.K. integral and Fraunhofer approximation, is written as follows [71]:

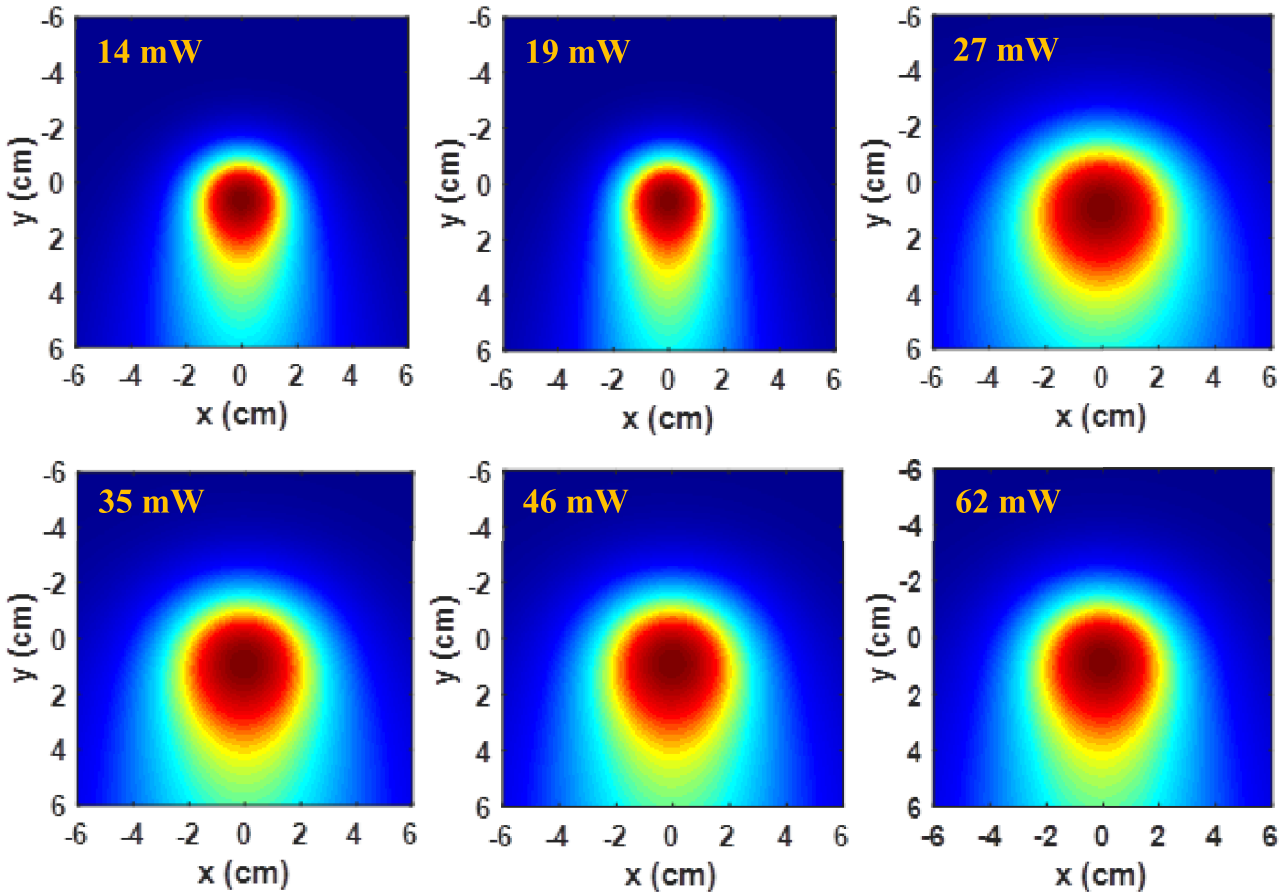

Fig. 16 Calculated results of 2-D variation of beam phase against input power in Sudan III solution

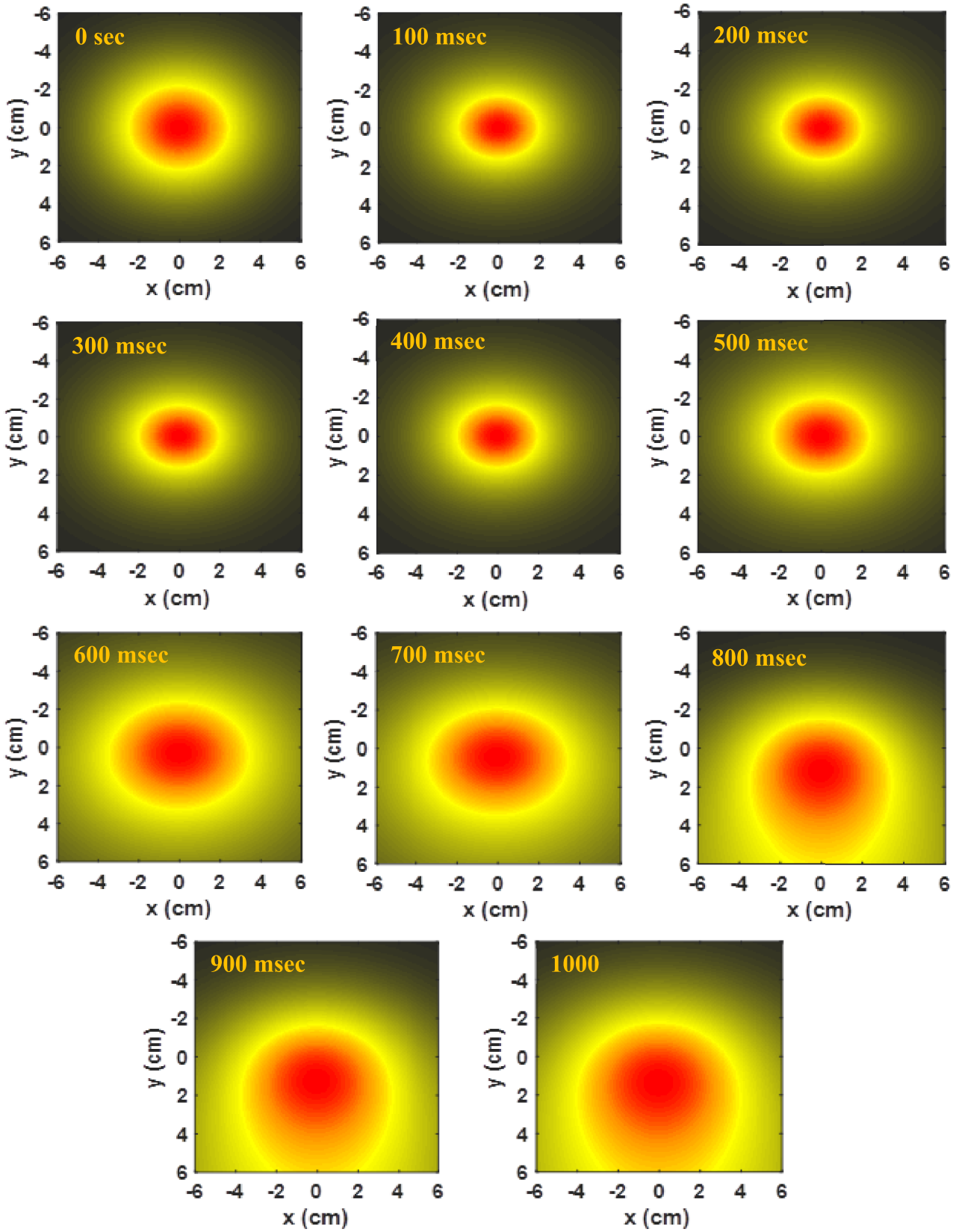

Fig. 17 Simulation results of temporal variation results of medium 2-D temperature at input power of 62 mW, in Sudan III solution

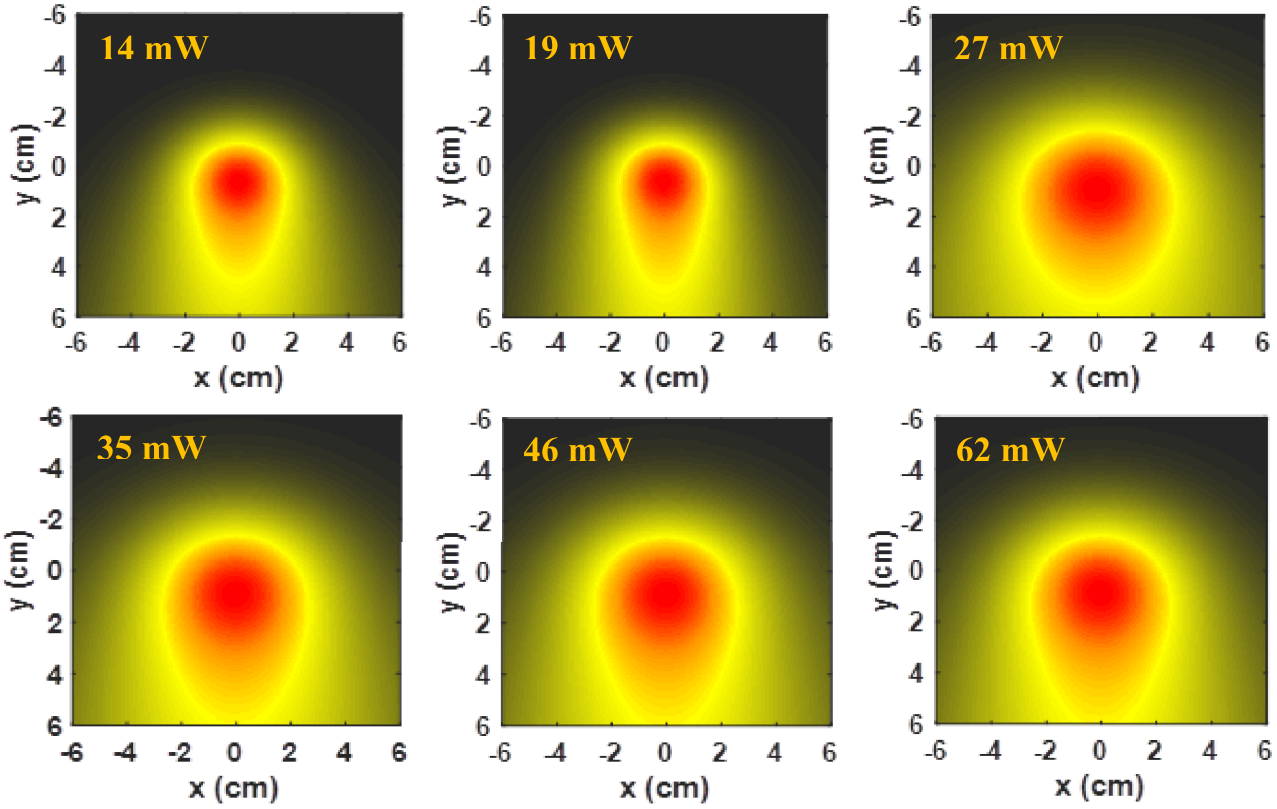

Fig. 18 Calculated results of 2-D variation of medium temperature against input power in Sudan III solution

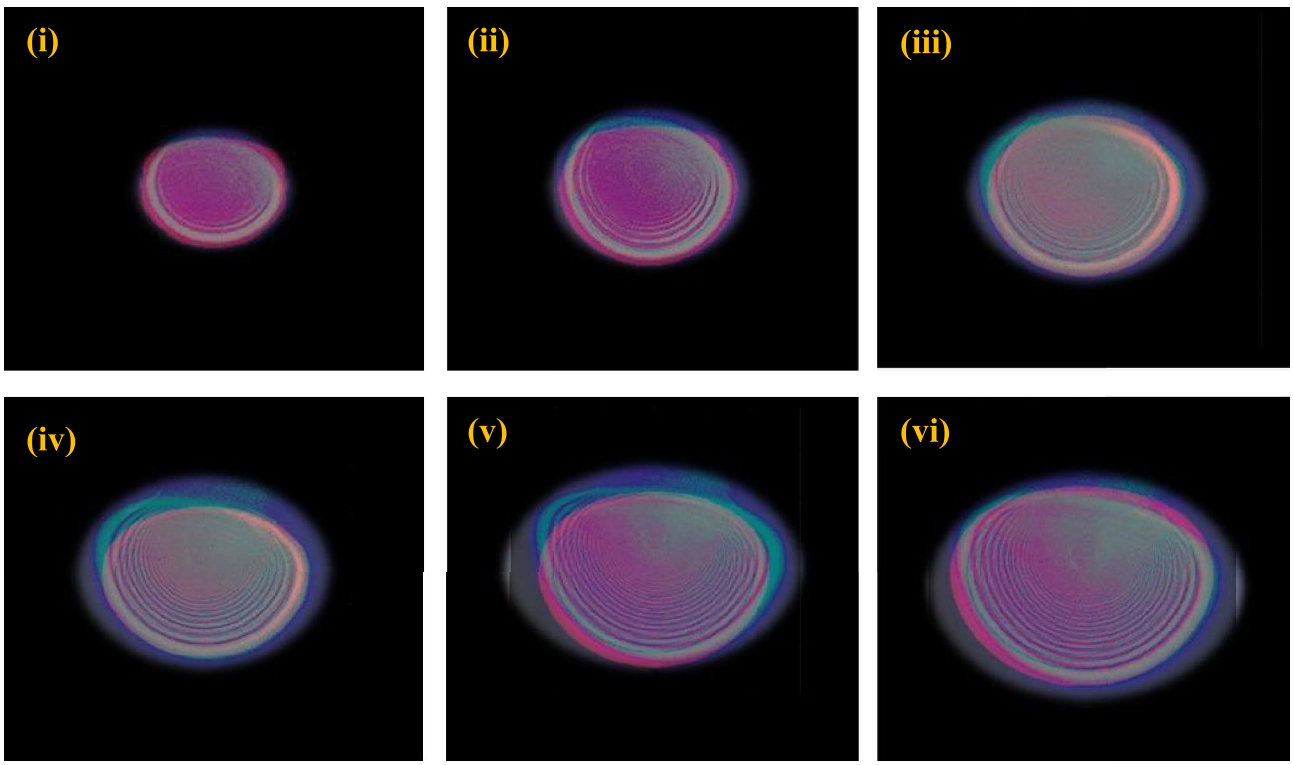

Fig. 19 Comparison of experimental (blue) as shown in Fig. 8 and simulated (red) chosen diffraction patterns (**i**) 14 mW, (**ii**) 19 mW, (**iii**) 27 mW, (**iv**) 35 mW, (**v**) 46 mW, (**vi**) 62 mW, in Sudan III

Table 1 Different materials NLRI, n_2, calculated via diffraction patterns and Z-scan by number of researchers

Materials	NLRI, n_2, cm^2/W	Method	Ref.
Absorbing solution	2.9×10^{-5}	DPs	[56]
Mercury diathizonate in polymer film	5.5×10^{-12}	DPs	[57]
Erioglaucine	$10^{-7}-10^{-6}$	DPs	[58]
Acid dye (patent green)	4.075×10^{-7}	DPs	[59]
Alcohol	20.53×10^{-8}	DPs	[60]
Acid green 25	6.23×10^{-7}	Z-scan	[61]
Acid blue 3 dye	5.71×10^{-7}	Z-scan	[62]
Triarylmethane dye	4.21×10^{-7}	Z-scan	[63]
Disperse blue 14 dye	2.96×10^{-7}	Z-scan	[64]

$$I\left(x',y',t\right)=|(\frac{2P}{\pi\omega^2})^{\frac{1}{2}}\frac{i\pi\omega^2}{\lambda L}\exp(ikL)\exp\left(-\frac{\alpha d}{2}\right)\int_{-\infty}^{\infty}dx\int_{-\infty}^{\infty}dy.\exp\left(-\frac{x^2+y^2}{\omega^2}\right).\exp[i\left(-k\frac{x^2+y^2}{2R}\right)+\Delta\varphi(x,y,t)].\exp\left(-ik\frac{xx'+yy'}{L}\right)|^2 \quad (6)$$

L is sample – screen distance.

Equation (6) was solved with a numerical scheme based on the Mat Lab system. The results of the calculations are shown in Figs. (13, 14, 15, 16, 17, 18). Figure 3 are the simulation results of temporal behavior of the DPs in 2D and intensity distribution against x and y axes and Fig. 14 shows the evolution of DPs against input power and intensity distribution against x and y axes. Figures 15 and 16 shows the calculations results of 2D temporal variations of the beam phase at 62 mW and it's 2D variations against input power in Sudan III solution respectively. Figures 17 and 18 shows the simulation results of 2D temporal variations of medium temperature and it's 2D variations against input power in Sudan III solution respectively. Comparison of the theoretical (red) and experimental (blue) DPs against power input are shown in Fig. 19.

Conclusion

This paper presents series of experimental and theoretical studies concerning the diffraction patterns that resulted when 473 nm, cw, visible laser beam traversed through Sudan III dye. The thermal properties of the Sudan III dye have been studied via obtaining the thermal conductivity and its relation with the dye temperature and in the diffraction patterns. The property all-optical switching in the Sudan III dye was tested using two laser beams viz., 473 and 635 nm and it was found that the Sudan III dye behave well during the test. Static and dynamic all-optical switching have been tested. High nonlinear refractive index, n_2, value of $7.693\text{x}10^{-6}$ cm^2/W was obtained.

Authors' Contributions Amir Hussein Ali participated in the characterization and analysis of the results, H. A. Sultan wrote the software program and manuscript, Qusay M.A. Hassan wrote the manuscript, C. A. Emshary wrote the main manuscript text – review & editing.

Availability of Data and Materials The authors confirm that the data supporting the findings of this study are available within the article.

Declarations

Ethics Approval and Consent to Participate The authors declare that their commitment to ethics related to his work and they have designed the experiments, collected and analyzed the data, and written the manuscript.

Consent for Publication The authors declare their consent of publication.

Conflict of Interests The authors declare that they have no known competing financial interests or personal relationships that could have appeared to influence the work reported in this paper.

References

1. Saeed BA, Hassan QMA, Emshary CA, Sultan HA, Elias RS (2020) The nonlinear optical properties of two dihydropyridones derived from curcumin. Spectrochim Acta Part A: Mol Biomol Spectrosc 240:118622 ((**1**4 pp)
2. Almashal FA, Mohammed MQ, Hassan QMA, Emshary CA, Sultan HA, Dhumad AM (2020) Spectroscopic and thermal nonlinearity study of a Schiff base compound. Opt Mater 100:109703 (12 pp)
3. Jassem AM, Hassan QMA, Emshary CA, Sultan HA, Almashal FA, Radhi WA (2021) Synthesis and optical nonlinear properties performance of azonaphthol dye. Phys Scr 96:025503 (20 pp)
4. Sultan HA, Dhumad AM, Hassan QMA, Fahad T, Emshary CA, Raheem NA (2021) Synthesis, characterization and the nonlinear optical properties of newly synthesized 4-(1,3-dioxo-1-phenylbutan-2-yl)diazenyl) benzenesulfonamide, Spectrochim. Acta, Part A: Mol. Biomol Spectrosc 251:119487 (15 pp)
5. Mutlaq DZ, Hassan QMA, Sultan HA, Emshary CA (2021) The optical nonlinear properties of a new synthesized azo-nitrone compound. Opt Mater 113:110815 (13 pp)
6. Elias RS, Hassan QMA, Emshary CA, Sultan HA, Saeed BA (2019) Formation and temporal evolution of diffraction ring patterns in a newly prepared dihydropyridone. Spectrochim Acta Part A: Mol Biomol Spectrosc 223:117297 (16 pp)
7. Dhumad AM, Hassan QMA, Emshary CA, Fahad T, Raheem NA, Sultan HA (2021) Nonlinear optical properties investigation of a newly synthesised Azo-(β)- diketone dye. J Photochem Photobio A: Chem 418:113429 (17 pp)
8. Dhumad AM, Hassan QMA, Fahad T, Emshary CA, Raheem NA, Sultan HA (2021) Synthesis, structural characterization, and optical nonlinear properties of two azo- β-diketones. J Mol Str 1235:130196 (9 pp)

9. Jassem AM, Hassan QMA, Almashal FA, Sultan HA, Dhumad AM, Emshary CA, Albaaj, L T T (2021) Spectroscopic study, theoretical calculations, and optical nonlinear properties of amino acid (glycine)-4-nitro benzaldeyhyde-derived Schiff base. Opt Mater 122:111750 (17 pp)
10. Abdullmajed HA, Sultan HA, Al-Asadi RH, Hassan QMA, Ali AA, Emshary CA (2022) Synthesis, DFT calculations and optical nonlinear properties of two derived Schiff base compounds from ethyl-4-amino benzoate. Phys Scr 97:025809 (18 pp)
11. Hassan DA, Sultan HA, Al-Asadi RH, Hassan QMA, Emshary CA, Fahad T (2022) DFT calculation and nonlinear optical properties of (E)-(2)-(8-hydroxyquinolin-5yl)diazenyl)-5-sulfamoylpheneyl)mercury (II) chloride. Phys B 639:413908 (13 pp)
12. Faisal AG, Hassan QMA, Alsalim TA, Sultan HA, Kamounah FS, Emshary CA (2022) Synthesis, optical nonlinear properties, and all-optical switching of curcumin analogues. J Phys Org Chem e4401:1–16
13. Al-Hujaj HH, Hassan QMA, Almashal FA, Sultan HA, Dhumad AM, Jassem AM, Emshary CA (2022) Benzenesulfonamide-thiazole system bearing an azide group: synthesis and evaluation of its optical nonlinear responses. Optik 265:169477 (16 pp)
14. Salim JK, Hassan QMA, Jassem AM, Sultan HA, Dhumad AM, Emshary CA (2022) An efficient ultrasound-assisted CH3COONa catalyzed synthesis of thiazolidinone molecule: theoretical and nonlinear optical evaluations of thiazolidinone-Schiff base derivative. Opt Mater 133:11291712
15. Khalaf SK, Hassan QMA, Emshary CA, Sultan HA (2022) Concentration effect on optical properties and optical limiting of PVA doped with nigrosin films. J Photochem Photob A: Chem 427:113809 (11 pp)
16. Wang J, Fiebig M (1996) Determination of the thermal diffusivity of aqueous solutions of methanol in an extended range of temperature by a laser-induced thermal grating technique. Exp Ther Flu Sci 13:38–43
17. Pilla V, Andrade AA, Lima SM, Catunda T, Donatti DA, Vollet DR, Ruiz AI (2003) spectroscopic and thermal characterization in poly (p-phenylene vinyle)/sol-gel silica sample. Opt Mater 24:483–489
18. Frumar M, Jedelsky J, Frumarova B, Wagner T, Hrdlicka M (2003) Optically and thermally induced changes of structure, linear and nonlinear optical properties of chalcogenides thin films. J Non-cryst Sol 326 and 327:399–404
19. Santhi A, Namboodiri VV, Radhakrishnan P, Nampoori V, P N (2006) Simultaneous determination of nonlinear optical and thermos-optic parameters of liquid samples. Appl Phys Lett 89(3):231113
20. Pilla V, Chillcce EF, Neves AAR, Munin E, Catunda T, Cesar CL, Barbosa LC (2007) Thermal-lens study of thermos-optical properties of tellurite glass. J Mater Sci 42:2304–2308
21. Pilla V, Munin E, Gesualdi M, R R(200) Measurment of the thermos-optic coefficient in liquids by laser-induced conical diffraction and thermal lens techniques, J Opt A: Pure Appl Opt 11:105201 (7pp)
22. Anari JZ, Karimzadeh R, Mansour N (2001) Optic properties and nonlinear rsponses of copper nanoparticles in polysiloxane oil. J Opt 12(9):025212
23. Dhanuskodi S, Girisun TCS, Bhagavannara-yana G, Uma S, Philip J (2011) Mechanical, thermal and laser damage threshold analysis of II group metal complexes of thiourea. Mater Chem Phys 126:463–469
24. Carvalho EA, Carmo AP, Bell MJV, Anjos V, Kassab LRP, da Silva DM (2012) Optical and thermal investigation of GeO2-PbO thin films doped with au and ag nanoparticles. Thin Sol Films 520:2667–2671
25. Sivakumar PK, Sagadevan S (2016) Studies on growth, spectral, thermal, mechanical and optical properties of 4-Bromo anilinium 4-Methylbenzeesulfonate crystal: a third order nonlinear optical material. Mater Res 19:937–941
26. Sun Z, Xu L, Chen Z, Wang Y, Tusilime K, Chang C, Zhao S, Li Y, Yu M, Zhang H (2019) Enhancing the mechanical and thermal properties of epoxy resin via blending with thermoplastic polysulfone. Polymers 11:461
27. Sadrolhosseini AR, Habibiasr M, Shafie S, Solaimani H, Lim HN (2019) Optical and thermal properties of laser-ablated platinum nanoparticles graphene oxide composite. Int J Molecu Sci 20:6153
28. Jeyaram S (2021) Study of third–order nonlinear optical properties of Basic Violet 3 Dye in polar protic and aprotic solvents. J Fluo 31:1637–1644
29. Sudha N, Surendran R, Jeyaram S (2022) Synthesis, spectral, solvent dependent linear and nonlinear optical characteristics of (E)-N-(3-(3-(4(dimethylamino) phenyl) acryloyl) pheny) quinolone-2-carboxamide. J Fluo 32:1471–1480
30. Jeyaram S (2022) Nonlinear optical responses in organic dye by Z-scan method. J Opt 51:666–671
31. Sudha N, Surendran R, Jeyaram S (2023) Low power Z-scan studies of Schiff base (E)-N'-(4-(dimethylamino) benzylidene) isonicotinohydrazide for nonlinear optical applications, accepted to publishing in Ind. J Phys. https://doi.org/10.1007/s12648-023-02764-2
32. Kadhum AJ, Hussein NA, Hassan QMA, Sultan HA, Al-Asadi AS, Emshary CA (2018) Investigating the nonlinear behavior of cobalt (II) phthalocyanine using visible CW laser beam. Optik 157:540–550
33. Hassan QMA, Sultan HA, Al-Asadi AS, Kadhum AJ, Hussein NA, Emshary CA (2019) Synthesis, characterization, and study of the nonlinear optical properties of two new organic compounds. Synth Met 257:116158(14 pp)
34. Hassan QMA, Raheem NA, Emshary CA, Dhumad AM, Sultan HA, Fahad T (2022) Preparation, DFT and optical nonlinear studies of a novel azo-(β)- diketone dye. Opt Las Technol 148:107705 (14 pp)
35. Al-Hamdani UJ, Hassan QMA, Zaidan AM, Sultan HA, Hussain KA, Emshary CA, Alabdullah, Z T Y (2022) Optical nonlinear properties and all optical switching in a synthesized liquid crystal. J Molec Liq 361:119676 (13 pp)
36. Raheem NA, Hassan QMA, Dhumad AM, Sultan HA, Fahad T, Emshary CA, Ali NW (2023) DFT structural and optical nonlinear investigations of a synthesized new azo β-diketone dye. J Ind Chem Soci. 100:100928(11 pp)
37. Moker MH, Hassan QMA, Ibraheem HS, Sultan HA, Dhumad AM, Emshary CA (2023) Synthesis, 2D-NMR analysis, DFT, and optical nonlinear studies of a new cyclic imide. J Molec Stru 1278:13492310
38. Issa MAR, Moker MH, Sultan HA, Dhumad AM, Hassan QMA, Emshary CA (2023) Synthesis, two dimensional NMR analysis, DFT, and nonlinear optical investigations of a new cyclic imide. J Molec Liq 379:121696 (12 pp)
39. Un-Nisa A, Zahra N, Butt YN (2016) Sudan dyes and their potential health effects. Pak J Biochem Mol Biol 49:29–35
40. Jabber WH, Hassan QMA, Al-Saymari FA (2023) Evaluation of surface roughness, linear and nonlinear optical parameters of a mixture of sudan black b and polymer films for optical limiting application. Optik 283:170938
41. Jabber WH, Hassan QMA, Al-Saymari FA (2023) Determination of Linear. Nonlinear, and the Optical limiting Properties of Sudan Brown RR in a solid Film and Solution, accepted to publishing in J Fluo. https://doi.org/10.1007/s10895-023-03227-x
42. Al-Timimy KhA, Hassan QMA, Sultan HA, Emshary CA (2020) Solvents effect on the optical nonlinear properties of the Sudan IV. Optik 224:165398

43. Zidan MD, Allaf AW, Ajji Z, Allaham A (2010) Optical limiting behavior of Sudan III dye doped polymer. Opt Las Technol 42:531–533
44. Asme A, Sagdinc SG (2013) The vibrational studies and theoretical investigation of structure, electronic and nonlinear optical properties of Sudan III [1-{[4- (phenylazo) phenyl]azo}-2-naphthalenol]. J Molecu Struc 1048:185–195
45. Taunaumang H, Dumais RX, Pondang J (2014) Characteristics of Sudan III-poly(N vinylcarbazole) composite film for optical sensor application. The J Technol Sci 25:91–98
46. Abbas B, Salman YT (2015) Study of photo-induced dichroism in Sudan III doped in poly(methylethacrylate) thin films. Acta Phys Polo 127:780–786
47. Taunaumang H, Poluakan C, Tambuwun A (2018) Investigation of physical structure of Sudan III film composite exposure to acetone, and alcohol vapor by using XRD method, IOP conf. Series: J Phys 1120 012060 (9pp)
48. Taunaumang H, Tuladi D, Wakary P (2021) Physical structure analysis and optical properties of Sudan III thin film. Adv Mater Phy Chem 11:101–110
49. Jia Y, Shan Y, Wu L, Dai X, Fan D, Xiang Y (2018) Broadband nonlinear optical resonance and all-optical switching of liquid phase exfoliated tungsten diselenide. Photo Res 5:1040–1047
50. Wang Q, Wu X, Wu L, Xiang Y (2019) Broadband nonlinear optical response in Bi2Se2-Bi2Te3 heterostructure and its application in all-optical switching. AIP Adv 9:025022
51. Zhang XJ, Yuan ZH, Yang RX, He Y, Qin YL, Si X, Jun H (2019) A review on spatial self-phase modulation of two dimensional material. J Cent South Univ 26:2295–2306
52. Muldiani RF, Hadiningrum K, Pratama D (2021) Experiments for determining the thermal conductivity of brass and 304 stainless steel with direct temperature measurement techniques using lorenz number as validation. Adv Engin Res 207:123–129
53. Nelkon M, Parker P (1988) Advanced Level Physics, 3rd Edition, Heinman London, pp 336–338
54. Price DM, Jarratt M (2002) Thermal conductivity of PTFE and PTFE composites. Thermochimica acta 392–393:231–236
55. Abu-El-Fadl A, Mohamad GA, El-Moiz AB, Rashad M (2005) Optical constants of $Zn_{1-x}Li_xO$ films prepared by chemical bath deposition technique. Phys B 366:44–54
56. Ogusu K, Kohtani Y, Shao H (1996) Laser-induced diffraction rings from an absorbing solution. Opt Rev 3:232–234
57. Yang X, Qi S, Zhang C, Chen K, Liang X, Yang G, Xu T, Han Y, Tian J (2005) The study of self-diffraction of mercury dithizonate in polyer film. Opt Commun 256:414–421
58. Ara MHM, Salmani S, Esmaeil-zadeh M, Mousavi SH, Koushki E, Shakouri K (2009) Optical characterization of erioglancine using Z-scan technique, beam radius variations and diffraction pattern in far-field. Curr Appl Phys 9:885–889
59. Ara MHM, Salmani S, Mousavi SH, Koushki E (2010) Investigation of nonlinear optical responses and observing diffraction rings in acid dye (patent green), Curr. Appl Phys 10:997–1001
60. Zhang Q, Cheng X, He B, Ren Z, Zhang Y, Chen M (2018) Investigation on thermally-induced optical nonlinearity of alcohols. Opt Las Technol 102:140–146
61. Jeyaram S, Geethakrishnan T (2017) Third-order nonlinear optical properties of acid green 25 dye by Z-scan method. Opt Las Technol 89:179–185
62. Jeyaram S, Geethakrishnan T (2020) Solvent Dependent Linear and Nonlinear Optical characteristics of Acid Blue 3 Dye. J Fluo 30:1161–1169
63. Jeyaram S (2021) Intermolecular charge transfer in donor–acceptor substituted triarylmethane dye for NLO and optical limiting applications. J Mater Sci Mater 32:9368–9376
64. Jeyaram S, Hemalatha S, Geethakrishnan T (2020) Nonlinear refraction, absorption and optical limiting properties of disperse blue 14 dye. Chem Phys Lett 739:137037
65. Agrawal GP (1987) Modulation instability induced by cross-phase modulation. Phys Rev Lett 59:880–883
66. Mckinstrie CJ, Russell DA (1988) Nonlinear focusing of coupled waves. Phys Rev Lett 61:2929–2932
67. Agrawal GP (1988) Population pulsations and nondegenerate four-wave mixing in semiconductor lasers and amplifiers. J Opt Soc Am B 5:147–158
68. Agrawal GP (1990) Induced focusing of optical beams in self-defocusing nonlinear media. Phys Rev Lett 64:2487–2490
69. Matsuoka S, Miyanaga N, Amano S, Nakatsuoka N (1997) Frequency modulation controlled by cross-phase modulation in optical fiber. Opt Lett 22:25–27
70. Jones DJ, Diddams SA, Taubman MS, Cundiff SJ, Ma LS, Hall JL (2000) Frequency comb generation using femtosecond pulses and cross-phase modulation in optical fiber at arbitrary center frequencies. Opt Lett 25:308–310
71. Karimzadeh R (2012) Spatial self-phase modulation of a laser beam propagation through liquids with self-induced natural convection flow. J Opt 14(9):095701